Corrosion Science 227 (2024) 111757

Contents lists available at ScienceDirect

Corrosion Science

journal homepage: www.elsevier.com/locate/corsci

Short Communication

Superior corrosion resistance of a slurry FeAl coating on 316LN stainless steel in 550 ℃ liquid lead-bismuth eutectic

Wen Wang [a], Zhaoguang Zhu [b], Liujie Yang [a], Jintao Lu [c], Jinyang Huang [c], Jibo Tan [b,*], Wenjun Kuang [a,*]

[a] Center for Advancing Materials Performance from the Nanoscale (CAMP-Nano), StateKey Laboratory for Mechanical Behaviorof Materials, Xian Jiaotong University, Xi'an 710049, China
[b] CAS Key Laboratory of Nuclear Materials and Safety Assessment, Institute of Metal Research, Chinese Academy of Sciences, Shenyang 110016, China
[c] National Energy R&D Center of Clean and High-Efficiency Fossil-Fired Power Generation Technology, Xi'an Thermal Power Research Institute Co., Ltd., Xingqing Road No.136, Xi'an, Shaanxi Province 710032, China

ARTICLE INFO

Keywords:
Fe-Al coating
Liquid metal corrosion
Passive films
Thermodynamics
STEM
XPS

ABSTRACT

An intermetallic Fe-Al coating was successfully produced on 316LN austenite stainless steel by slurry Aluminizing. The coating greatly enhanced the corrosion resistance of substrate in LBE (lead-bismuth eutectic) containing low (10^{-7} wt%) and high (1.8×10^{-3} wt%) oxygen concentrations at 550 ℃ and the coating was mostly intact after 1500 h exposure test. The high corrosion resistance results from the formation of a uniform layer of alumina oxide on the coating which can be achieved when the dissolved oxygen is above 10^{-18} wt%. This FeAl coating maybe a promising option for protecting structure material in the fourth LBE-cooled fast reactor.

1. Introduction

Lead-bismuth eutectic (LBE: 44.5 wt% Pb, 55.5 wt% Bi) is considered a promising coolant in Gen-IV nuclear power reactors due to its high thermal conductivity, excellent neutron properties and good compatibility with air and water [1–3]. However, it can lead to degradations of structural materials, such as liquid metal corrosion (LMC) and liquid metal embrittlement (LME), which pose a significant limitation on its widespread application [4–6].

Austenitic stainless steels (SSs) (e.g. 316 L SS, 15–15Ti, 1.4571) have been extensively studied as candidate structural materials for LBE-cooled fast reactors due to their general good corrosion resistance [7–9]. However, the presence of highly soluble elements such as Ni and Mn can result in significant dissolution of structural materials when the dissolved oxygen (DO) concentration in LBE is low [6,10]. The selective dissolution of metallic elements not only leads to material loss with LBE ingress but also causes ferritization of the dissolution-affected zone [11–14]. The ingress of LBE into material is closely linked to the embrittlement of material. Moreover, under high DO concentration, severe oxidation can occur [15–18]. This leads to the formation of a bilayer oxide structure (an outer layer of magnetite and an inner layer of Fe-Cr spinel) on the surface of material which degrades the heat transfer ability and load bearing capacity of structure materials.

To mitigate dissolution and oxidation of structural materials in LBE, various approaches have been proposed, including oxygen control and surface modification. One promising approach is the deposition of a protective coating on the substrate [19]. Several types of coatings have been proposed and examined in LBE, such as ceramic coating (TiN, TiAlN, Al_2O_3, Ti_3ScC, etc) [20–23] and metallic coating (FeAl, CrAl, FeCrAl, FeCrAlY, AlCrFeMoTi, etc) [24–28] which have shown good corrosion resistance to LBE. The ceramic coating exhibits high hardness, good wear resistance and high thermal stability, but lacks self-healing ability and enough ductility [19]. By comparison, the metallic coating has good bonding strength with the matrix and a passivation film can form on its surface due to the addition of active elements (such as Al and Cr) which significantly improves the corrosion resistance to LBE.

G. Müller et al. reported that Fe-Al coating on austenite stainless steel showed good corrosion resistance to LBE even at 600 ℃ after 2000 h exposure as a stable thin alumina layer formed [24]. J Yang et al. evaluated the performance of a high entropy alloy (HEA) AlCrFeMoTi coating and the result indicated that a thin and dense oxide layer formed and effectively protected the coating and matrix against the LBE attack at 550 ℃ [28]. The metallic coatings exhibited good corrosion resistance in LBE because the formed oxide films can efficiently prevent LBE from

* Corresponding authors.
E-mail addresses: jbtan10s@imr.ac.cn (J. Tan), wjkuang66@gmail.com (W. Kuang).

https://doi.org/10.1016/j.corsci.2023.111757
Received 21 August 2023; Received in revised form 22 November 2023; Accepted 6 December 2023
Available online 10 December 2023
0010-938X/© 2023 Elsevier Ltd. All rights reserved.

Table 1
Chemical composition of 316LN SS (wt%).

Element	Cr	Ni	Si	Mo	Mn	N	P	C	S	Fe
Content	16.92	12.92	0.35	2.08	1.37	0.12	0.018	0.015	<0.003	Balance

contacting the material directly. Nevertheless, the coating's thickness decreases gradually as the passive film forms and degrades [4]. More importantly, the above studies only examined the corrosion resistance of coating in LBE with a single oxygen concentration and the reliability of these coatings remains questionable in a wide range of DO concentration.

This work investigated the effect of an aluminide coating formed via slurry aluminizing [29] on the corrosion resistance of austenitic stainless steel in LBE. The performance of such coating was fully evaluated in 550 ℃ LBE with high and low oxygen concentrations (i.e. oxygen-saturated (1.8×10^{-3} wt%) and oxygen-poor (10^{-7} wt%) conditions). The details of oxygen control can be found in a previous work [30]. Further microscopic analysis was conducted to clarify the excellent LBE corrosion resistance of the aluminide coating.

2. Experiment

316 LN SS rectangular coupons (30 mm × 11 mm×3 mm) with a chemical composition as shown in Table 1 were prepared for aluminide coating. These specimens were ground with silicon carbide papers up to 1200 grit and then ultrasonically cleaned in acetone before the coating procedure.

Slurry aluminizing was used to form aluminide coating. The detailed process can be found in previous works [29,31]. The slurry used for

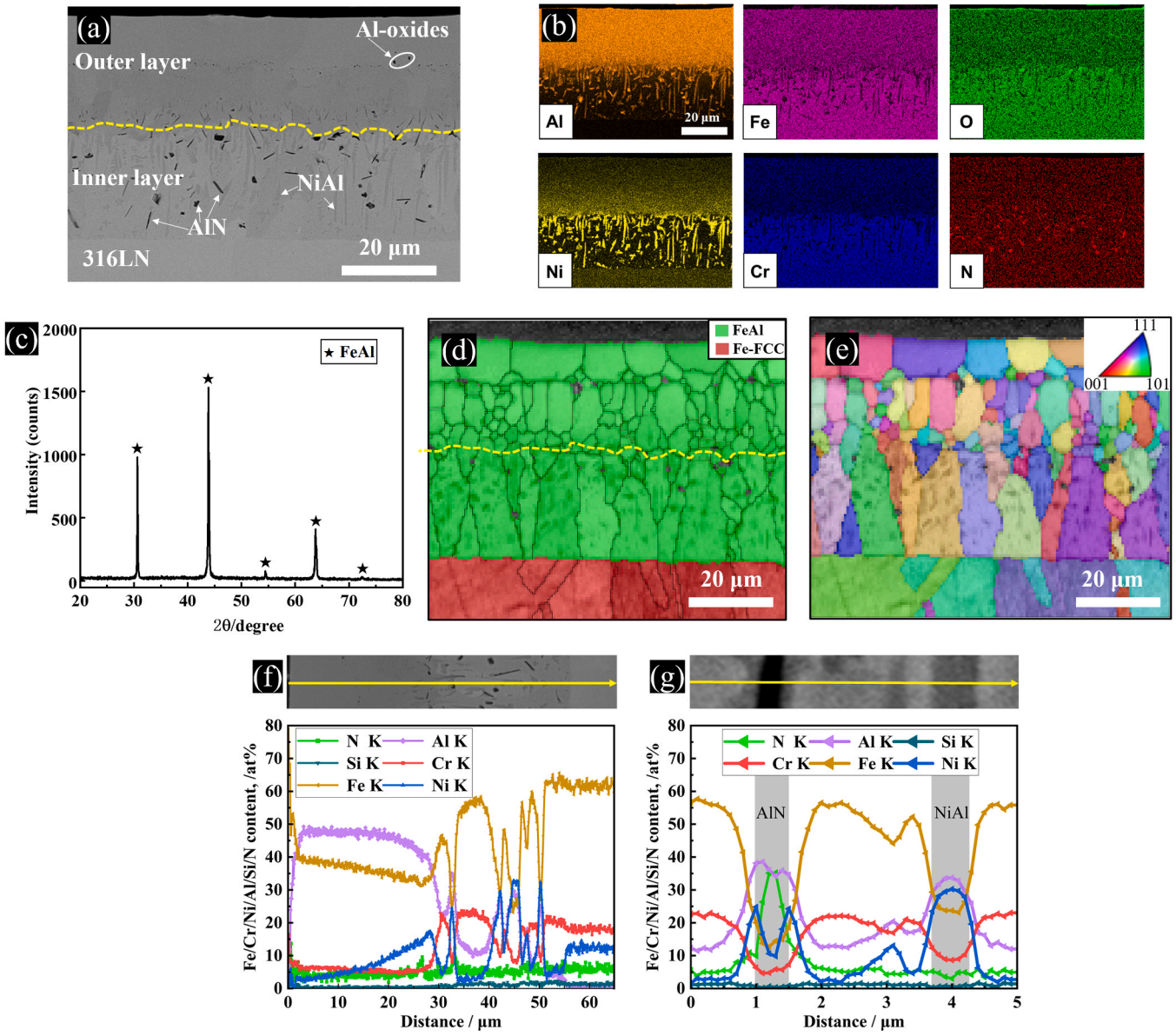

Fig. 1. (a) SEM-BSE image of coating cross-section. (b) SEM-EDS mapping of coating cross-section. (c) XRD pattern of coating surface. (d-e) EBSD analysis of the coating cross-section: (d) Band contrast+Phase, (e) Band contrast+Inverse pole figure. (f) EDS line scan of coating cross-section. (g) EDS line scan of AlN and NiAl precipitates.

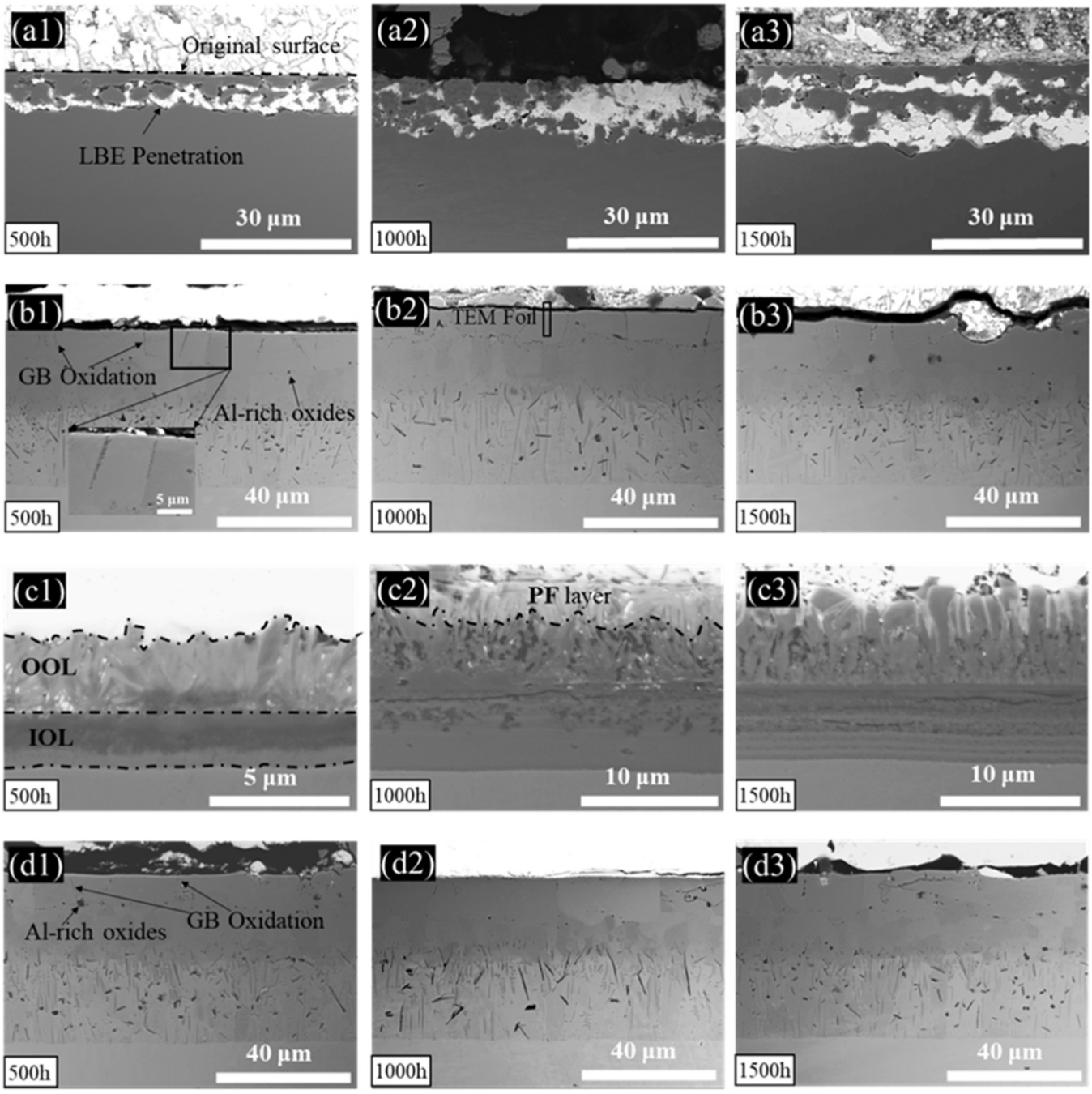

Fig. 2. (a1-a3) SEM-BSE images of 316LN SS after exposure tests in oxygen-poor LBE: (a1) 500 h, (a2) 1000 h, (a3) 1500 h. (b1-b3) SEM-BSE images of coated samples after exposure tests in oxygen-poor LBE: (b1) 500 h, (b2) 1000 h, (b3) 1500 h. (c1-c3) SEM-BSE images of 316LN SS after exposure tests in oxygen-saturated LBE: (c1) 500 h, (c2) 1000 h, (c3) 1500 h. (d1-d3) SEM-BSE images of coated samples after exposure tests in oxygen-saturated LBE: (d1) 500 h, (d2) 1000 h, (d3) 1500 h.

coating contains approximately 50–60% Al, 20–30% Si, 10–20% Ni, 5–8% Al_2O_3 and 2–5% activator (by mass). Si serves as a co-dopant to facilitate Al infiltration into the substrate. A SiO_2 layer was formed on the surface after the aluminizing process which was then removed. The slurry was sprayed onto the surface of 316LN SS specimens, resulting in a slurry thickness of approximately 0.2 mm. Subsequently, the sprayed specimens were dried at 200 ℃. The process of aluminizing was thermally activated at 980 ℃ in argon atmosphere and lasted for 5 h, followed by cooling in air. The coated coupons were cleaned three times with alcohol.

The LBE corrosion tests of as-coated and raw materials were carried out in a static LBE corrosion system as in a previous work [30]. The corrosion time ranged from 500 to 1500 h and two oxygen concentrations (oxygen-saturated: 1.8×10^{-3} wt% and oxygen-poor: 10^{-7} wt%) were used. A Pt/air electrode sensor was used to measure the DO concentration in LBE. After exposure test, some specimens were cleaned with a solution containing acetic acid, ethanol and hydrogen peroxide (the volume ratio is 1:1:1) to remove residual LBE on the surface. Some specimens were cut by diamond wire carefully and then cold mounted with epoxy resin. The cold mounted specimens were mechanically ground up to 3000 grit with silicon carbide papers and then vibration polished in 0.05 μm alumina suspension to remove the surface deformation layer.

The phase structure of the as-coated specimen was analyzed in an X-

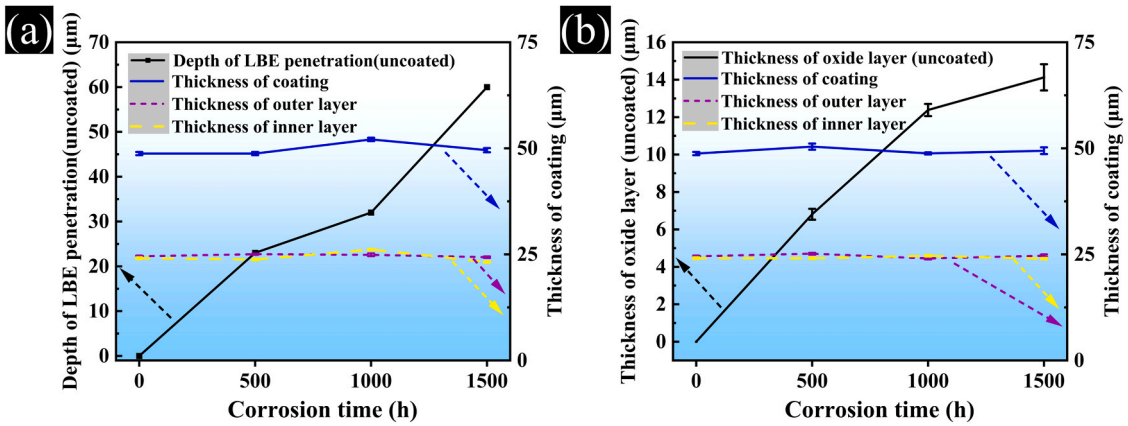

Fig. 3. (a) The thickness of coating (including inner and outer layer) and the maximum penetration depth of lead-bismuth (uncoated sample) with time in oxygen-poor LBE. (b) The thicknesses of coating (including inner and outer layer) and the oxide layer formed on the substrate (uncoated sample) with time in oxygen-saturated LBE.

ray diffractometer (Bruker D8 ADVANCE). A Zeiss Gemini 500 equipped with an electron back-scattered diffraction (EBSD) detector was used to examine the cross-section of as-coated specimen. Chemical and microstructural characterizations were performed with a Hitachi SU6600 scanning electron microscopy (SEM) with X-ray energy-dispersive spectroscopy (EDAX Octane SDD) and back-scattered electron (BSE) detectors. The TEM lamella of corroded coated specimen (after exposure to oxygen-poor condition for 1000 h) was prepared in a Hitachi NX5000 Focused Ion Beam (FIB) system. The FIB lamella was analyzed using a JEOL JEM-F200 (HR) Transmission Electron Microscopy (TEM) with two 100 mm^2 EDS detectors and a high angle annular dark-filed (HAADF) detector. An X-ray photoelectron spectroscopy (Thermo Fisher ESCALAB Xi+) was used to measure the chemical composition of coated specimens after LBE corrosion.

3. Results and discussion

The cross-section morphology of as-coated 316LN SS is shown in Fig. 1a. The coating shows a double-layer structure and the thickness of initial coating is 48.8 ± 0.38 μm. From the corresponding EDS mappings (Fig. 1b), the outer layer mainly contains Al and Fe while the inner layer is rich in Fe and Cr. The Cr content in the inner layer is slightly higher than in the substrate. That is because the original FCC Fe-Cr-Ni substrate transformed into BCC Fe-Cr solid solution due to the loss of Ni and some redundant Cr diffused to this layer. The BSE image indicates the presence of dark particles in the outer layer which were identified as Al oxide according to the EDS mappings. In the inner layer, the EDS mappings and the EDS line scan (Fig. 1g) reveal the presence of numerous vertical strip-like precipitates which is probably the NiAl phase as reported before [32]. Moreover, AlN precipitates were also observed, displaying both strip-like and granular shapes [33]. From the EDS line scan of the cross-section of the coating (Fig. 1f), there is a sharp change in the content of Fe and Al elements at the interface between the inner and outer layers of the coating. During the aluminizing process, Al gradually infiltrated the substrate and formed B_2 phase with Fe and Ni. Meanwhile, some Al diffused to the inner layer and formed precipitates with Ni and N. As Ni diffused to the outer layer, the original Fe-Cr-Ni austenite transformed to Fe-Cr ferrite in the inner layer. Redundant Cr also diffused to the inner layer. Phase structure analysis of the coating (Fig. 1c) was carried out with XRD diffraction which indicates that β-FeAl (B_2 structure) is the dominant phase in the outer layer. The EBSD analysis (Fig. 1d) shows that the coating and the matrix have body-centered cubic (BCC) structure and face-centered cubic (FCC) structure, respectively. The nearly straight boundary between the coating and the substrate indicates that the Al infiltration process was quite uniform. The grain morphology varies from equiaxed to columnar shape from the outer to inner layer. That is probably related to the directional diffusion flux. The diffusion flux from the substrate is nearly perpendicular to the sample surface. Hence, the growth rate of coating is fastest along this direction, resulting in columnar grain shape. For the outer coating layer, the original columnar grains would gradually change to equiaxed ones so as to decrease the total grain boundary energy. Besides, the inverse pole figure (Fig. 1e) shows that the crystallographic orientations of columnar grains are randomly distributed with no preferential relationship with the substrate grains.

The SEM morphologies of cross-section of all specimens after different exposure tests in 550 °C LBE with two oxygen concentrations are shown in Fig. 2. The cross-sections of 316LN SS matrix after exposure test in oxygen-poor LBE (Fig. 2(a1-a3)) show that LBE penetrated into the matrix and some cavities formed within the LBE penetrated area. The cavities may be caused by the dissolution of Ni and Mn into LBE [34]. It is worth noting that due to the extremely low S content (<0.003 wt%) in 316LN stainless steel, MnS did not form and the cavity formation should not be related to it. The cross-section images of coated coupons after exposure test in oxygen-poor LBE (Fig. 2(b1-b3)) show that the coating was mostly intact, indicating much improved resistance to LBE attack. At this magnification, no obvious oxide film was observed on the coating. Although some grain boundaries were oxidized in the outer layer of coating, the overall coating structure was still maintained and no obvious spallation was observed across the entire cross-section. The coating still maintains its double-layer structure. The outer layer structure remains relatively intact and the inner layer also shows a significant amount of precipitates. From the morphology and composition (not shown here) of the precipitates in the inner layer, it can be concluded that the precipitates are the same as those in the original coating, i.e. NiAl and AlN precipitates. Thus, the coating exhibits high stability after 1500 h exposure to oxygen-poor LBE at 550 °C.

Fig. 2(c1-c3) show the cross-section of 316LN SS after exposure in oxygen-saturated LBE. The oxide film shows a typical bilayer structure, mainly composed of an outer oxide layer (OOL) and an inner oxide layer (IOL). The bilayer structure has been well reported before (the OOL is mainly Fe_3O_4 and the IOL is (Fe, Cr, Ni)$_3O_4$ spinel [35,36]). It is worth noting that above the bilayer oxide, there is a loose layer on the surface (Fig. 2(c2)). According to the previous study, this layer is mainly composed of iron-lead composite oxides (plumboferrite, PF), which was formed through the reaction of Fe and Pb with dissolved oxygen in LBE [37]. The thickness of oxide layer gradually increased with increasing exposure time. For the coated samples exposed to oxygen-saturated LBE, the cross-sections (Fig. 2(d1-d3)) show that the coating also remained intact although some intergranular oxidation occurred (insert in Fig. 2 (b1)). Despite the higher DO concentration, an oxide layer was not clearly observed on the coating at the current magnification either. The

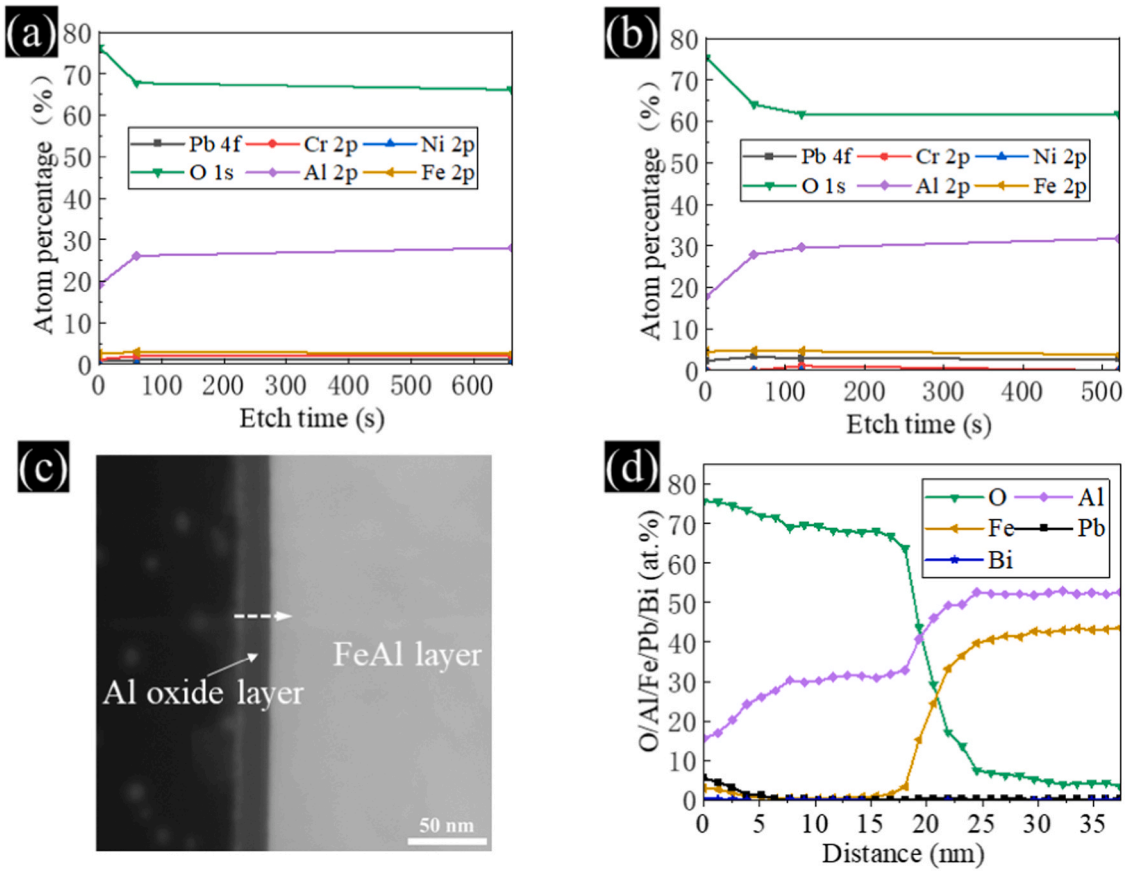

Fig. 4. (a-b). XPS profiles of coated 316LN SS after exposure to LBE: (a) oxygen-poor LBE for 1000 h, (b) oxygen-saturated LBE for 1000 h. (c) STEM-HADDF image of TEM foil sampled in Fig. 2(b2), (d) EDS line scan along the dash line in (c).

coating did not undergo significant changes in structure or composition either after exposure to oxygen-saturated LBE, confirming its excellent stability and corrosion resistance.

The measurements of maximum penetration depth of LBE, the thicknesses of oxide layer and residual coating (outer layer, inner layer and overall coating) are presented in Fig. 3. The maximum penetration depth of LBE was measured from an 11 mm long cross-section. The oxide layer or coating was sectioned at 3 μm intervals across a length of about 300 μm from the cross-section. The average oxide or coating thicknesses was then obtained in each section by dividing the area of oxidation or coating by interval size. Finally, the overall averages of oxide and coating thicknesses and standard deviations were calculated from those section averages. After the exposure tests in oxygen-poor LBE (Fig. 3a), the thickness of coating shows minimal changes compared to the original state. The thickness of coating after 1000 h exposure in oxygen-poor LBE appears thicker than the others, which could be due to the variations in the initial thickness of coating among different samples. The overall thickness of the original coating was maintained around 50 μm. Also, there is little change in the thicknesses of the inner and outer layers after LBE corrosion, indicating that the coating exhibits high stability in 550 °C oxygen-poor LBE corrosion environment. In contrast, the maximum depth of LBE penetration into the un-coated substrate increased significantly over time. The maximum penetration depth reached 60 μm after 1500 h-exposure. Similar situation was also observed after tests in oxygen-saturated LBE (Fig. 3b). There was no significant change in the thickness of coating (including inner and outer layers) either while the thickness of oxide layer on the un-coated substrate gradually increased with increasing corrosion time. The increase rate of oxide layer thickness decreases over time, indicating that the formed oxide layer could decrease the oxidation rate of substrate to some extent [38–40].

The coated samples after 1000 h-exposure in LBE were further cleaned to remove residual LBE from the surface. Subsequently, XPS measurement with sputtering was carried out on the cleaned surface to acquire the elemental composition. The XPS measurements (Fig. 4a and b) confirm that the formed surface oxide mainly contains O and Al, indicating that the Al-rich oxide layer formed on the coating surface regardless of the oxygen content in LBE. TEM characterization was further performed on a FIB lift-out fabricated from the cross-section of the sample exposed to oxygen-poor LBE for 1000 h (the lift-out position is shown in Fig. 2(b2)). The STEM-HAADF image (Fig. 4c) reveals the presence of a compact and uniform oxide layer on the coating surface. From the EDS line profile along the white dashed line in Fig. 4c, Al and O are the main elements in the surface oxide layer. Additionally, there are weak signals of Fe and Pb in the outermost layer with a penetration depth of a few nm. Thus, it is confirmed that an alumina layer could form on the coating surface during exposure to LBE and acted as an effective barrier layer.

Based on the SEM-EDS results, the Al content of the coating varies from 39 to 57 at%. So we assume that the Al content is 45 at% for the convenience of thermodynamic calculation and the activity of Al in Fe-45Al can be estimated. The activity of Al in FeAl alloy system was calculated in previous studies [41,42] and the difference in Al activity between different temperatures can be expressed as:

$$\log\left(\alpha_{Al}\right)_2 - \log\left(\alpha_{Al}\right)_1 = \frac{\Delta\bar{H}_{Al}}{4.575}\left(\frac{1}{T_2} - \frac{1}{T_1}\right) \quad (1)$$

Where T_2 and T_1 are the absolute temperatures, $(\alpha_{Al})_2$ and $(\alpha_{Al})_1$ are the activities of Al at T_2 and T_1. $\Delta\bar{H}_{Al}$ is the relative partial molar enthalpy of Al. In this study, $\Delta\bar{H}_{Al}$ is − 32.44 kJ/mol [43]. Eldridge et al. have reported that α_{Al} in Fe-45Al is 0.0256 at 1173 K [42]. Based on Eq. (1), Al

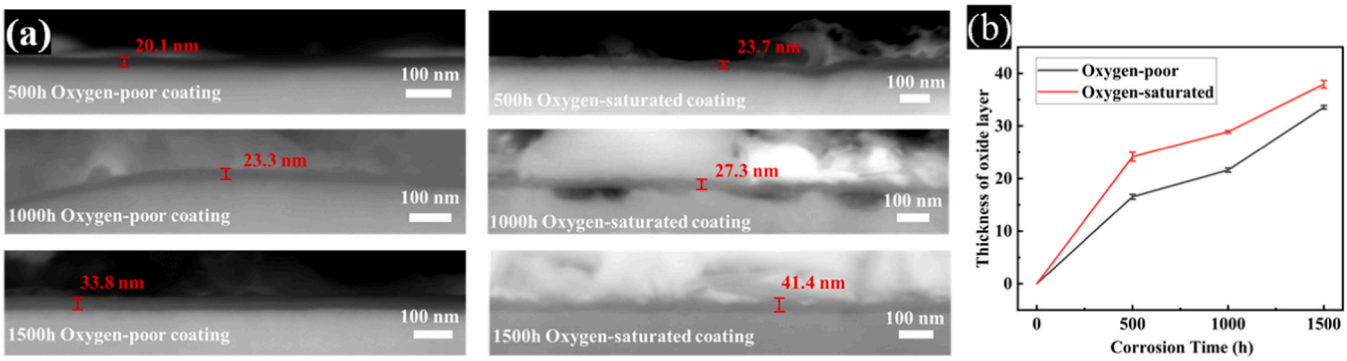

Fig. 5. (a) Typical high-magnification SEM-BSE images of the alumina layer on the coating after LBE corrosion. (b) Statistical results of the thickness of the alumina layer.

activity in Fe-45Al at 550 °C was calculated to be 6.88×10^{-5}.

To calculate the critical oxygen partial pressure to form alumina, the following equations can be established by assuming the activity of Al oxide equals 1 [41]:

$$\frac{4}{3}Al + O_2 = \frac{2}{3}Al_2O_3 \quad \Delta G^0 = -1077381 + 185.4T\ (J) \tag{2}$$

$$P_{O_2} = (\alpha_{Al})^{-\frac{4}{3}} \times \exp\left(\frac{\Delta G^0}{RT}\right) \tag{3}$$

Where ΔG^0 is the change in standard Gibbs free energy, R is the gas constant, α_{Al} is the activity of Al, P_{O2} is the equilibrium partial pressure of oxygen which can be converted to DO concentration in LBE based on Eq. (4) [44]:

$$P_{O_2} \Big/ bar = C_O^2 \exp\left(13.558 - \frac{32005}{T}\right) \tag{4}$$

By calculation, the critical DO concentration required to form stable Al_2O_3 on Fe-45Al at 550 °C is $10^{-18.57}$ wt%, much lower than the used oxygen concentrations. Therefore, formation of Al_2O_3 is thermodynamically favorable under both conditions, which is also consistent with the results observed in the experiment. According to the previous results [28,45], Al_2O_3 film can serve as stable barrier against LBE corrosion. That is why the coated 316 LN SS was intact after exposure to LBE.

To statistically analyze the thickness of oxide layer grown on the coatings, we imaged the cross-sections of the corroded coatings in SEM-BSE mode at high-magnification. Fig. 5(a) shows typical high-magnification images of the oxide layer on coating after LBE corrosion. A nanoscale oxide film covers the surface of the corroded coating and the thickness of oxide layer is less than 50 nm. The average thickness of oxide layer from a 100 μm wide section was measured for each sample, as shown in Fig. 5(b). Under oxygen-poor condition, the thickness of oxide layer is generally smaller than that under oxygen-saturated condition. After 1500 h, the average oxide layer thickness under oxygen-poor condition is 33.5 nm, while it is 37.9 nm under oxygen-saturated condition. Such difference could be attributed to a higher thermodynamic driving force for the formation of alumina film and thus a faster growth rate in LBE with higher DO concentration.

Based on the above experimental results and thermodynamic calculations, it is concluded that alumina layer can form on the surface of FeAl coating and is able to greatly enhance the corrosion resistance against the attack of LBE within a wide range of oxygen concentration. Moreover, slurry coating technique can be easily applied to component with complex geometry and the metallurgical bonding between coating and substrate normally possesses high strength. These merits may make the slurry FeAl coating a promising surface treatment technique for protecting structure material used in LBE-cooled fast reactor.

4. Conclusion

In this study, a slurry aluminide coating was successfully produced on a 316LN SS substrate. The coating mainly contains FeAl phase, with a non-uniform microstructure transitioning from outer equiaxed grains to inner columnar grains. After static LBE corrosion tests at 550 ℃ under two different dissolved oxygen concentrations (oxygen-poor (10^{-7} wt%) and oxygen-saturated (1.8×10^{-3} wt%)), the coating demonstrated excellent resistance to LBE corrosion compared to the uncoated 316LN SS substrate. The thickness of coating remained constant and the coating structure was almost intact. It was confirmed that a thin layer of alumina film formed on the surface of coating after exposure to LBE regardless of the used oxygen concentrations. The formation of alumina on FeAl is thermodynamically favorable in 550 ℃ LBE when the dissolved oxygen concentration is above 10^{-18} wt%. Therefore, it is concluded that the slurry Fe-Al coating can provide good corrosion resistance to LBE attack at 550 ℃ within a wide range of dissolved oxygen concentration and maybe used to protect structure materials used in LBE-cooled fast reactor.

CRediT authorship contribution statement

Lu Jintao: Data curation, Methodology, Funding acquisition. **Yang Liujie:** Data curation, Investigation. **Zhu Zhaoguang:** Data curation, Investigation. **Wang Wen:** Data curation, Investigation, Methodology, Visualization, Writing – original draft, Writing – review & editing. **Kuang Wenjun:** Conceptualization, Data curation, Funding acquisition, Investigation, Methodology, Project administration, Supervision. **Tan Jibo:** Investigation, Methodology, Project administration, Supervision, Funding acquisition. **Huang Jinyang:** Data curation, Methodology, Funding acquisition.

Declaration of Competing Interest

The authors declare that they have no known competing financial interests or personal relationships that could have appeared to influence the work reported in this paper.

Data availability

The raw/processed data required to reproduce these findings cannot be shared at this time as the data also forms part of an ongoing study.

Acknowledgements

The authors gratefully acknowledge the financial supports from Innovation Center of Nuclear Materials, China Atomic Energy Authority (No. ICNM-2022-YZ-03) and National Natural Science Foundation of China (No. 52271070). The authors thank Jiao Li, JiaWei Wang and

Chenyu Liang at Instrument Analysis Center of Xi'an Jiaotong University for their assistance with TEM, SEM and XPS analysis, Xiaohua Cheng, Chaowei Guo and Pengcheng Zhang at Center for Advancing Materials Performance from the Nanoscale (CAMP-Nano) of Xi'an Jiaotong University for their assistance with SEM and FIB analysis and Wei Wang at Experimental Technology Center of Materials Science and Engineering of Xi'an Jiaotong University for his assistance with SEM analysis.

References

[1] C. Fazio, Handbook on Lead-bismuth Eutectic Alloy and Lead Properties, Materials Compatibility, Thermal-hydraulics and Technologies: 2015 Edition - Introduction, OECD, 2016.
[2] T.R. Allen, D.C. Crawford, Lead-cooled fast reactor systems and the fuels and materials challenges, Sci. Technol. Nucl. Install. 2007 (2007), 097486.
[3] P. Lorusso, S. Bassini, A. Del Nevo, I. Di Piazza, F. Giannetti, M. Tarantino, M. Utili, GEN-IV LFR development: status & perspectives, Prog. Nucl. Energy 105 (2018) 318–331.
[4] X. Gong, M.P. Short, T. Auger, E. Charalampopoulou, K. Lambrinou, Environmental degradation of structural materials in liquid lead- and lead-bismuth eutectic-cooled reactors, Prog. Mater. Sci. 126 (2022), 100920.
[5] J. Zhang, N. Li, Review of the studies on fundamental issues in LBE corrosion, J. Nucl. Mater. 373 (2008) 351–377.
[6] J. Zhang, A review of steel corrosion by liquid lead and lead–bismuth, Corros. Sci. 51 (2009) 1207–1227.
[7] E. Stergar, S.G. Eremin, S. Gavrilov, M. Lambrecht, O. Makarov, V. Iakovlev, Influence of LBE long term exposure and simultaneous fast neutron irradiation on the mechanical properties of T91 and 316L, J. Nucl. Mater. 473 (2016) 28–34.
[8] X. Gong, Z. Yang, Y. Deng, J. Xiao, H. Wang, Z. Yu, Y. Yin, Creep failure of a solution-annealed 15-15Ti steel exposed to stagnant lead-bismuth eutectic at 550 and 600 °C, Mater. Sci. Eng. A 798 (2020), 140230.
[9] V. Tsisar, C. Schroer, O. Wedemeyer, A. Skrypnik, J. Konys, Corrosion behavior of austenitic steels 1.4970, 316L and 1.4571 in flowing LBE at 450 and 550°C with 10−7mass% dissolved oxygen, J. Nucl. Mater., 454 (2014) 332–342.
[10] A. Heinzel, A. Weisenburger, G. Müller, Corrosion behavior of austenitic steels in liquid lead bismuth containing 10−6wt% and 10−8wt% oxygen at 400–500°C, J. Nucl. Mater. 448 (2014) 163–171.
[11] E. Charalampopoulou, K. Lambrinou, T. Van der Donck, B. Paladino, F. Di Fonzo, C. Azina, P. Eklund, S. Mráz, J.M. Schneider, D. Schryvers, R. Delville, Early stages of dissolution corrosion in 316L and DIN 1.4970 austenitic stainless steels with and without anticorrosion coatings in static liquid lead-bismuth eutectic (LBE) at 500 °C, Mater. Charact. 178 (2021), 111234.
[12] E. Charalampopoulou, N. Cautaerts, T. Van der Donck, D. Schryvers, K. Lambrinou, R. Delville, Orientation relationship of the austenite-to-ferrite transformation in austenitic stainless steels due to dissolution corrosion in contact with liquid Pb-Bi eutectic, Scr. Mater. 167 (2019) 66–70.
[13] P. Hosemann, D. Frazer, E. Stergar, K. Lambrinou, Twin boundary-accelerated ferritization of austenitic stainless steels in liquid lead–bismuth eutectic, Scr. Mater. 118 (2016) 37–40.
[14] C. Schroer, O. Wedemeyer, J. Novotny, A. Skrypnik, J. Konys, Selective leaching of nickel and chromium from Type 316 austenitic steel in oxygen-containing lead–bismuth eutectic (LBE), Corros. Sci. 84 (2014) 113–124.
[15] H. Wang, H. Yu, J. Liu, S. Kondo, N. Okubo, R. Kasada, Characterization and corrosion behavior of Al-added high Mn ODS austenitic steels in oxygen-saturated lead–bismuth eutectic, Corros. Sci. 209 (2022), 110818.
[16] O. Yeliseyeva, V. Tsisar, G. Benamati, Influence of temperature on the interaction mode of T91 and AISI 316L steels with Pb–Bi melt saturated by oxygen, Corros. Sci. 50 (2008) 1672–1683.
[17] D. Wang, S. Liu, C. Xiao, X. Ma, Y. Sun, G. Yuan, J. Zeng, Y. Liang, Y. Hu, F. Niu, X. Gong, Corrosion resistance of 15–15Ti and 316Ti austenitic steels as fuel cladding in liquid lead-bismuth eutectic at 550 ℃: the dominant role of grain structure, Corros. Sci. 218 (2023), 111169.
[18] L. Martinelli, C. Jean-Louis, B.-C. Fanny, Oxidation of steels in liquid lead bismuth: oxygen control to achieve efficient corrosion protection, Nucl. Eng. Des. 241 (2011) 1288–1294.
[19] E. Serag, B. Caers, P. Schuurmans, S. Lucas, E. Haye, Challenges and coating solutions for wear and corrosion inside lead bismuth eutectic: a review, Surf. Coat. Technol. 441 (2022), 128542.
[20] Z.Y. Wu, X. Zhao, Y. Liu, Y. Cai, J.Y. Li, H. Chen, Q. Wan, D. Yang, J. Tan, H.D. Liu, Y.M. Chen, J.L. Guo, J. Zhang, G.D. Zhang, Z.G. Li, B. Yang, Lead-bismuth eutectic (LBE) corrosion behavior of AlTiN coatings at 550 and 600° C, J. Nucl. Mater. 539 (2020), 152280.
[21] H. Glasbrenner, F. Gröschel, Exposure of pre-stressed T91 coated with TiN, CrN and DLC to Pb–55.5Bi, J. Nucl. Mater. 356 (2006) 213–221.
[22] F.G. Ferré, A. Mairov, D. Iadicicco, M. Vanazzi, S. Bassini, M. Utili, M. Tarantino, M. Bragaglia, F.R. Lamastra, F. Nanni, L. Ceseracciu, Y. Serruys, P. Trocellier, L. Beck, K. Sridharan, M.G. Beghi, F. Di, Fonzo, Corrosion and radiation resistant nanoceramic coatings for lead fast reactors, Corros. Sci. 124 (2017) 80–92.
[23] A. Heinzel, A. Weisenburger, G. Müller, Long-term corrosion tests of Ti3SiC2 and Ti2AlC in oxygen containing LBE at temperatures up to 700 °C, J. Nucl. Mater. 482 (2016) 114–123.
[24] G. Müller, A. Heinzel, J. Konys, G. Schumacher, A. Weisenburger, F. Zimmermann, V. Engelko, A. Rusanov, V. Markov, Results of steel corrosion tests in flowing liquid Pb/Bi at 420–600 °C after 2000h, J. Nucl. Mater. 301 (2002) 40–46.
[25] E. Yamaki-Irisawa, S. Numata, M. Takahashi, Corrosion behavior of heat-treated Fe–Al coated steel in lead–bismuth eutectic under loading, Prog. Nucl. Energy 53 (2011) 1066–1072.
[26] R. Fetzer, A. Weisenburger, A. Jianu, G. Müller, Oxide scale formation of modified FeCrAl coatings exposed to liquid lead, Corros. Sci. 55 (2012) 213–218.
[27] A. Weisenburger, A. Heinzel, G. Müller, H. Muscher, A. Rousanov, T91 cladding tubes with and without modified FeCrAlY coatings exposed in LBE at different flow, stress and temperature conditions, J. Nucl. Mater. 376 (2008) 274–281.
[28] J. Yang, K. Shi, W. Zhang, Q. Chen, Z. Ning, C. Zhu, J. Liao, Y. Yang, N. Liu, W. Zhang, J. Yang, A novel AlCrFeMoTi high-entropy alloy coating with a high corrosion-resistance in lead-bismuth eutectic alloy, Corros. Sci. 187 (2021), 109524.
[29] J. Lu, J. Huang, J. Wang, Z. Yang, Y. Gu, Long-term degradation behavior of slurry aluminide coating on Super304H stainless steel at 650 °C, Corros. Sci. 178 (2021), 109054.
[30] Z. Zhu, Q. Zhang, J. Tan, X. Wu, H. Ma, Z. Zhang, Q. Ren, E.-H. Han, X. Wang, Corrosion behavior of T91 steel in liquid lead-bismuth eutectic at 550 °C: Effects of exposure time and dissolved oxygen concentration, Corros. Sci. 204 (2022), 110405.
[31] J. Lu, Y. Dang, J. Huang, Y. Zhou, Z. Yang, J. Yan, Y. Yuan, Y. Gu, Preparation and characterization of slurry aluminide coating on Super304H boiler tube in combination with heat-treatment process, Surf. Coat. Technol. 370 (2019) 97–105.
[32] Z. Yang, J.-t Lu, P. Zhang, M. Le, Y.-l Zhou, J.-y Huang, Y. Yuan, Y.-f Gu, Oxidation performance and degradation mechanism of the slurry aluminide coating deposited on Super304H in steam at 600–650 °C, Surf. Coat. Technol. 391 (2020), 125700.
[33] T.D. Nguyen, X. Peng, J. Zhang, D.J. Young, Corrosion resistance of chromised and aluminised coatings in wet CO_2 gas at 650°C, Surf. Coat. Technol. 316 (2017) 226–238.
[34] E. Yamaki, K. Ginestar, L. Martinelli, Dissolution mechanism of 316L in lead–bismuth eutectic at 500°C, Corros. Sci. 53 (2011) 3075–3085.
[35] D. Koury, A.L. Johnson, T. Ho, J.W. Farley, Analysis of bi-layer oxide on austenitic stainless steel, 316L, exposed to Lead–Bismuth Eutectic (LBE) by X-ray Photoelectron Spectroscopy (XPS), J. Nucl. Mater. 440 (2013) 28–33.
[36] C. Cionea, M.D. Abad, Y. Aussat, D. Frazer, A.J. Gubser, P. Hosemann, Oxide scale formation on 316L and FeCrAl steels exposed to oxygen controlled static LBE at temperatures up to 800°C, Sol. Energy Mater. Sol. Cells 144 (2016) 235–246.
[37] Q. Shi, J. Liu, H. Luan, Z. Yang, W. Wang, W. Yan, Y. Shan, K. Yang, Oxidation behavior of ferritic/martensitic steels in stagnant liquid LBE saturated by oxygen at 600°C, J. Nucl. Mater. 457 (2015) 135–141.
[38] L. Martinelli, F. Balbaud-Célérier, G. Picard, G. Santarini, Oxidation mechanism of a Fe-9Cr-1Mo steel by liquid Pb–Bi eutectic alloy (Part III), Corros. Sci. 50 (2008) 2549–2559.
[39] L. Martinelli, F. Balbaud-Célérier, A. Terlain, S. Delpech, G. Santarini, J. Favergeon, G. Moulin, M. Tabarant, G. Picard, Oxidation mechanism of a Fe–9Cr–1Mo steel by liquid Pb–Bi eutectic alloy (Part I), Corros. Sci. 50 (2008) 2523–2536.
[40] L. Martinelli, F. Balbaud-Célérier, A. Terlain, S. Bosonnet, G. Picard, G. Santarini, Oxidation mechanism of an Fe–9Cr–1Mo steel by liquid Pb–Bi eutectic alloy at 470°C (Part II), Corros. Sci. 50 (2008) 2537–2548.
[41] C.H. Xu, W. Gao, Y.D. He, High temperature oxidation behaviour of FeAl intermetallics—oxide scales formed in ambient atmosphere, Scr. Mater. 42 (2000) 975–980.
[42] J. Eldridge, K.L. Komarek, Thermodynamic properties of solid iron-aluminum alloys, Trans. Metall. Soc. AIME 230 (1964) 226.
[43] S.V. Radcliffe, B.L. Averbach, M. Cohen, Relative thermodynamic properties of solid iron-aluminum alloys, Acta Metall. 9 (1961) 169–176.
[44] C. Schroer, J. Konys, Physical Chemistry of Corrosion and Oxygen Control in Liquid Lead and Lead-bismuth Eutectic, in, Germany, 2007.
[45] A. Jianu, R. Fetzer, A. Weisenburger, S. Doyle, M. Bruns, A. Heinzel, P. Hosemann, G. Mueller, Stability domain of alumina thermally grown on Fe–Cr–Al-based model alloys and modified surface layers exposed to oxygen-containing molten Pb, J. Nucl. Mater. 470 (2016) 68–75.